Monodromy and chaos for condensed bosons in optical lattices

Geva Arwas[1,2], Doron Cohen[1]
[1] *Department of Physics, Ben-Gurion University of the Negev, Beer-Sheva 84105, Israel*
[2] *Department of Physics of Complex Systems, Weizmann Institute of Science, Rehovot 7610001, Israel*

We introduce a theory for the stability of a condensate in an optical lattice. We show that the understanding of the stability-to-ergodicity transition involves the fusion of *monodromy* and *chaos* theory. Specifically, the condensate can decay if a connected chaotic pathway to depletion is formed, which requires swap of seperatrices in phase-space.

Ergodicity, as opposed to Stability, is the threat that looms over the condensation of bosons in optical lattices. A major question of interest is whether an initial condensate is likely to be depleted. The simplest setup is the dimer, aka Bosonic Josephson Junction [1–3], where condensation in the upper orbital can become unstable if the interaction exceeds a critical value. A more challenging setup is a ring lattice [4–8], where the particles are condensed into an excited momentum orbital. If such flow-state is metastable, it can be regarded as a mesoscopic version of supefluidity. It has been realized that the theory for this superfluidity requires analysis that goes beyond the tradition framework of Landau and Bogoliubov, because the underlying dynamics is largely chaotic [9, 10].

The structure of the classical phase-space is reflected in the quantum spectrum, and provides the key for quantum-chaos theory of mesoscopic superfluity. In the present work we highlight the essential ingredient for the crossover from stability to ergodicity. We consider the minimal setup: a 3 site ring. We show that the understanding of this transition involves the fusion of two major research themes: *monodromy* and *chaos*.

Monodromy.– The dynamics of an integrable (non-chaotic) system, for a given value of the conserved constants-of-motion, can be described by a set of action-angle variables, that parametrize a torus in phase space. In systems with monodromy, they cannot be defined globally: due to the non trivial topology of phase space, the action-angle variables cannot be identified in a continuous way in the parameter-space that is formed by the conserved quantities [11, 12]. Accordingly, it is impossible to describe the quantum spectrum by a global set of good quantum numbers [13, 14]. Rather, the good quantum numbers (quantized "actions") that are implied by the EBK quantization scheme form a lattice that features a topological defect [15]. Such Hamiltonian monodromy is found in many physical systems, such as the spherical [13, 16] and the swing-spring [17, 18] pendula, Spin-1 condensed bosons [19], the Dicke model [20], and even the hydrogen atom [21]. A dynamical manifestation of monodromy in a classical system has been recently demonstrated [22].

Chaos.– The condensation of particles in a single orbital is a many-body coherent state. It can be represented in phase-space as a Gaussian-like distribution that is supported by a stationary point (SP). If this SP is the minimum of the energy landscape, it is known as Landau energetic stability, and leads, for a clean ring, to the Landau criterion for superfluidity. More generally one has to find the Bogoliubov excitations ω_r of condensate. If some of the frequencies become complex, the SP is considered to be unstable. What we have demonstrated in previous work [5, 10] was that this type of local stability analysis does not provide the required criteria for stability. Rather, in order to determine whether the system will ergodize, it is essential to study the global structure of phase-space, and to take into account the role of chaos.

Connectivity.– The major insight can be described schematically as follows. Let us regard the SP that supports the condensate as the *origin* of phase-space. And let us regard the region that supports the completely depleted states as the *perimeter* of phase-space. The crucial question is whether there is a dynamical pathway that leads from the origin to the perimeter. We have observed numerically in [10] that the formation of such pathway requires a swap of phase-space separatrices. But a theory for this swap transition has not been provided.

Outline.– In what follows we present the Hamiltonian of the system, and write it as the sum of integrable part $\mathcal{H}^{(0)}$, and additional terms $\mathcal{H}^{(\pm)}$ that induce the chaos. An example for the classical and quantum spectra is presented in Fig.1. The spectra exhibit monodromy that we analyze in detail: the quantum monodromy is a reflection of the classical one. Then we explain how the spectrum is affected by changing a control parameter (detuning). In an hysteresis experiment [23] the detuning is determined by the rotation frequency of the device and the interaction strength between the bosons. We provide a geometrical explanation for the *swap transition*, and clarify the role of chaos in the de-stabilization of the condensate.

Model.– The Bose-Hubbard Hamiltonian (BHH) is a prototype model for cold atoms in optical lattices that has inspired state-of-the-art experiments [24, 25]. Here we consider a 3-site ring with N bosons. Such ring has 3 momentum orbitals labeled by their wavenumber $k = 0, 1, 2$. Later we assume, without loss of generality, that the particles are initially condensed in the $k = 0$ orbital. This is not necessarily the ground-state orbital, because we allow the possibility that the ring is in a rotating frame. After some time the condensate

can be partially depleted such that the occupation is $(N-n_1-n_2, n_1, n_2)$. We have here a 2 freedom system whose Hamiltonian can be written in terms of canonical coordinates as [a]:

$$\mathcal{H}(\varphi, n; \phi, M) = \mathcal{H}^{(0)}(\varphi, n; M) + \left[\mathcal{H}^{(+)} + \mathcal{H}^{(-)}\right] \quad (1)$$

Here $n = (n_1 + n_2)/2$ and $M = (n_1 - n_2)/2$, and (φ, ϕ) are conjugate angle variables. The first term $\mathcal{H}^{(0)}$ is an integrable piece of the Hamiltonian that has M as an additional constant of motion:

$$\begin{aligned}\mathcal{H}^{(0)}(\varphi, n; M) \;&=\; \mathcal{E}n + \mathcal{E}_\perp M - \frac{U}{3}M^2 \qquad (2)\\ &+\frac{2U}{3}(N-2n)\left[\frac{3}{4}n + \sqrt{n^2 - M^2}\cos(\varphi)\right]\end{aligned}$$

where U is the interaction between the bosons, while the detuning $\mathcal{E}$ determines the energy difference between the condensate $(n = 0)$ and the depleted states $(n = N/2)$. If we linearized $\mathcal{H}$ with respect to the (n_1, n_2) occupations, we would get the Bogoliubov approximation, which is Eq. (2) without the third term (M^2), and with $(N-2n) \approx N$. The additional terms $\mathcal{H}^{(\pm)}$ induce resonances that spoil the integrability, and give rise to chaos.

$$\mathcal{H}^{(\pm)} = \frac{2U}{3}\sqrt{(N-2n)(n\pm M)}(n\mp M)\cos\left(\frac{3\phi\mp\varphi}{2}\right) \quad (3)$$

Stability.– The first impression is that $\mathcal{H}^{(0)}$ is very similar to the well-studied $\mathcal{H}_{\rm dimer}$ [a], that describes the dynamics of the bosonic Josephson junction. All we have to do is to rescale the occupation coordinate $\tilde{n} = 2n$. Without loss of generality we assume $\mathcal{E} > 0$. Then $\tilde{n} = 0$ corresponds to condensation in the lower mode, while $\tilde{n} = N$ corresponds to condensation in the upper mode. Both states are stationary points (SPs) of the Hamiltonian. In the dimer case the lower mode condensation is always *stable*, while the upper mode condensation becomes *unstable* if $\mathcal{E} < NU$ [b]. But for our 3 site ring Eq. (2) the stability analysis is more interesting: both SPs become unstable in the range $|\mathcal{E}| < (1/6)NU$ [b].

Geometry.– The stability analysis reflect the algebraic side of the dynamics, but ignores the geometrical aspect. The phase space of the dimer is the Bloch sphere. All the $(\tilde{\varphi}, \tilde{n}{=}0)$ points are in fact the same point, which can be regarded as the North pole of the sphere. Same applies to $(\tilde{\varphi}, \tilde{n}{=}N)$ which can be regarded as the South pole of the sphere. But for our 3 site ring Eq. (2) the geometry of phase-space is different. One difference is that the angle is folded $(\varphi = 2\tilde{\varphi})$. Accordingly the North pole, if unstable, is the cusp on a folded separatrix of half-saddle topography. As for the South pole, it is no longer a single point, because different φ values indicate different points in phase space. So in fact we no longer have a Bloch-sphere, but rather we have a Bloch-disc. The perimeter of the disc is a *spread SP*. If the spread SP becomes unstable, there is a seperatrix that comes out from the perimeter in an angle $\varphi_{\rm out}$, and comes back to it in an angle $\varphi_{\rm in}$. Both the approach and the departure from the perimeter along the separatrix require an extremely long time. We emphasize again that from an algebraic point of view the dynamics is the same as if the perimeter were a single point on a Bloch-sphere. The (φ, n) phase space structure is illustrated in Fig.2.

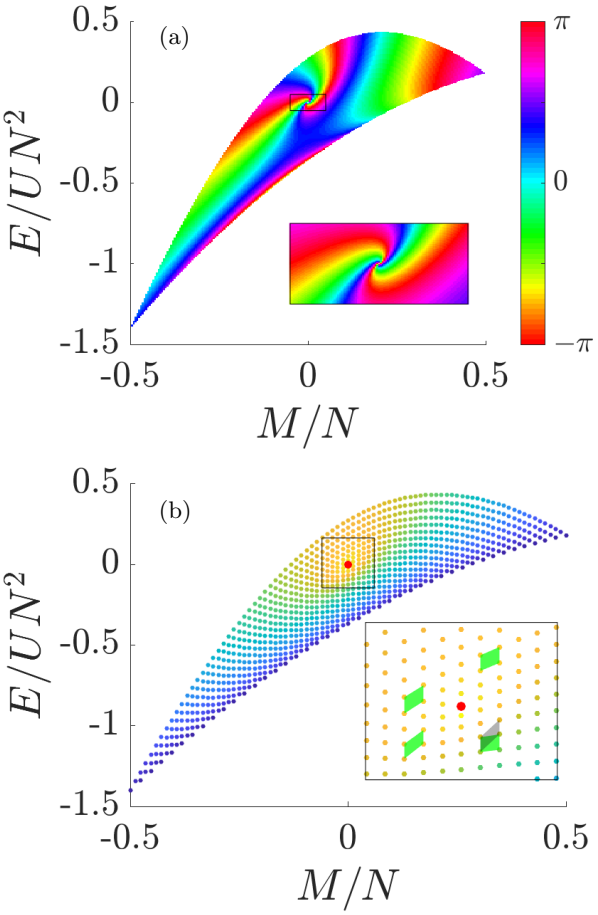

FIG. 1. **Monodromy.** The classical and quantum spectra of the Hamiltonian $\mathcal{H}^{(0)}$. This Hamiltonian has a constant of motion M, that describes the occupation imbalance of the $k \neq 0$ orbitals. In (a) each point represents an (M, E) torus in phase space, and the points are color coded by the value of a classical phase (β) that characterizes the torus. In (b) each point represent an $|M, E\rangle$ eigenstate of $N = 42$ particles, and the points are color coded by the expectation value of the variable n, which is the total occupation of the $k \neq 0$ orbitals. Yellow color $(n < N/8)$ indicates a nearly coherent condensate, while blue implies a depleted eigenstate. In both panels $\mathcal{E}/NU \approx -1/4$ and $\mathcal{E}_\perp/NU \approx 1/2$. The inset provides a zoom that demonstrates the monodromy: a topological defect in the lattice arrangement of the spectrum.

Topology.– So far we have discussed the one-freedom projected dynamics of (φ, n). But now we have to remember that there is an additional degree of freedom (ϕ, M). We consider the dynamics that is generated by

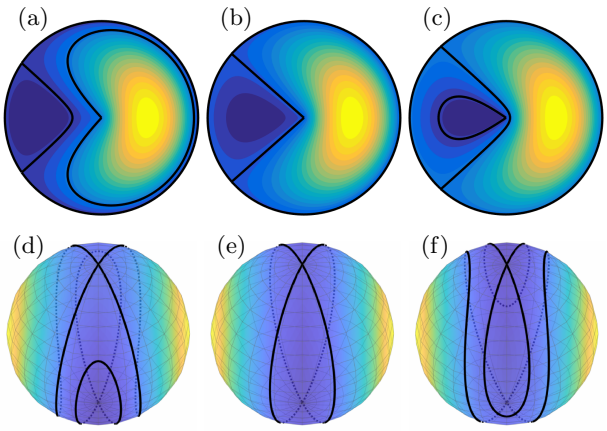

FIG. 2. **The geometry of the projected phase space.** Top panels: the (φ, n) disk. Bottom panels: the $(\tilde{\varphi}, \tilde{n})$ Bloch-sphere. The detuning is $\mathcal{E}/NU = -0.05, 0.00, 0.05$ (from left to right). The color stands for the energy. Black lines indicate the separatrices that go through the SPs. Here we focus in the parametric range where both SPs are unstable [b, c].

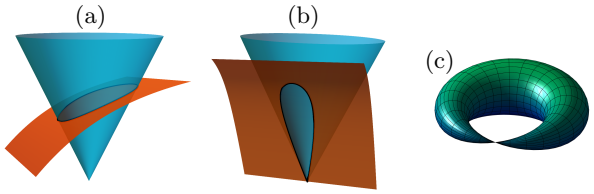

FIG. 3. **Phase space topology**. The blue cone is an $M = 0$ surface, that intersects with a surface of constant E. The existence of an additional coordinate (ϕ) at each point is implicit. The intersection is a torus. Panel (a) is the typical case, while (b) corresponds to a pinched torus (see text). The latter is fully illustrated (with ϕ) in panel (c).

$\mathcal{H}^{(0)}$, where M is a constant of motion, and the conjugate angle is doing circles with $\dot{\phi} = \partial\mathcal{H}/\partial M$. A trajectory that is generated by $\mathcal{H}^{(0)}$ covers a torus in phase space. A useful way for visualizing the tori is based on the $SU(1,1)$ symmetry [19, 26] of $\mathcal{H}^{(0)}$. The (φ, n) dynamics is the intersection of constant E and constant M surfaces, see Fig.3 [c]. In particular the $M = 0$ surface is a cone, whose tip corresponds to $n = 0$, while its outer boundary to $n = N/2$. If the intersection forms a closed loop, as in Fig.3a, the trajectory covers a torus in phase space. But if the trajectory goes through $n = 0$, as in Fig.3b, we get a *pinched torus*, see Fig.3c. This is because the ϕ-circle at $n = 0$ has zero radius. This "zero radius" is explained as follows: if $n = 0$ then necessarily $n_1 = n_2 = 0$, hence all the (φ, ϕ) angles degenerate, representing a single phase-space point.

Swap transition.– Recall that $\mathcal{E}$ is controlled experimentally by the rotation frequency of the device. Fig.2 shows how the two SPs of the projected dynamics are re-arranged as the detuning $\mathcal{E}$ changes sign. At the transition the two separatirces coalesce, thus forming connection between the origin (which supports the condensate) and the perimeter (where the k=0 orbital is completely depleted). Once the $\mathcal{H}^{(\pm)}$ terms are added, a connecting quasi-stochastic strip is formed, through which the initial state can decay. This is shown in Fig.4, where we plot a Poincare section of the full Hamiltonian Eq.(1). One should note the subtle relation between the perspective of Fig.4 and that of Fig.2. A panel of the latter displays sections of $M = 0$ tori that form a vertical subset in a Fig.1-type (M, E) diagram, while a panel of Fig.4 displays sections of same E trajectories that form a horizontal subset of such diagram. The pinched torus is contained in both subsets.

Away from the swap transition, the chaotic region around $n = 0$ is bounded by the surviving Kolmogorov-Arnold-Moser (KAM) tori, forming a *chaotic pond* which is isolate from the perimeter region. Hence the depletion of the condensate is arrested. It is only in the vicinity of the swap transition that a connected chaotic pathway to depletion is formed. Thus, a local stability analysis of the SP using the standard Bogoliubov procedure does not provide the proper criterion for superflow metastability.

Quantization.– The classical structure of phase-space is reflected in the many-body spectrum. If chaos is ignored the eigenstates can be labeled by the good quantum numbers that are determined by the commuting operators M and $\mathcal{H}^{(0)}$, as in Fig.1b. If we add the $\mathcal{H}^{(\pm)}$ terms we can still order the energies according to the expectation value $\langle M \rangle$. Several examples are provided in Fig.5 [d]. For presentation purposes, the perimeter energy $E_x(M)$, which corresponds to maximum depleted state ($n = N/2$), is taken as the reference.

From a semiclassical perspective, if we ignore the chaos, each point can be associated with an EBK torus [e]. Namely, the "good quantum numbers" are quantized values of the action variables. The lattice arrangement of the energies in Fig.1b reflects the way that the tori are embedded in phase-space, while the chaos, once added, blurs it locally, see Fig.5. This lattice arrangement is supported by a classical skeleton that is formed by a pinched torus (marked by a red dot), and an $E = E_x(M)$ separatrix. At the vicinity of the separatrix the spectrum is dense, reflecting that the frequency of the motion goes to zero. Irrespective of that, the quantum spectrum has a topological defect that is described by a monodromy (to be further discussed below). This monodromy reflects the presence of the pinched torus. The sequence of panels in Fig.5 shows how the swap transition is reflected in the quantum spectrum. This transition happens as the red dot, which corresponds to the pinched torus, crosses the $E = E_x$ separatrix line. We see how the yellow condensation region is diminished at the transition.

Monodromy calculation.– The concept of monodromy is pedagogically summarized in [e]. For our model system, in the absence of chaos, we have in in-

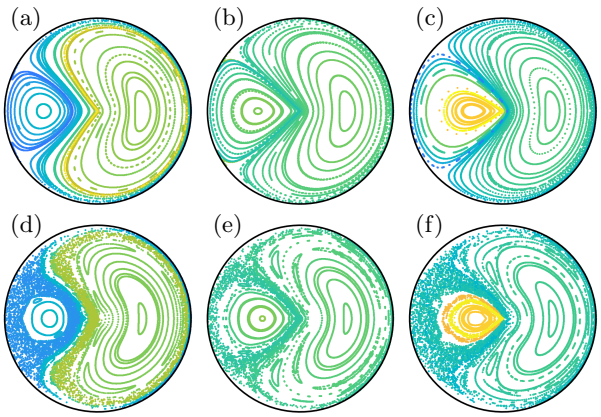

FIG. 4. **Poincare sections.** The dynamics of the full Hamiltonian Eq.(1) projected to the (φ, n) disk. All the trajectories are launched with the same energy as that of the condensate. The left to right arrangement of the panels is by detuning $(\mathcal{E}/NU)$, in one-to-one correspondence with Fig.2. In the upper panels the interaction strength is $NU \sim 1$, in units of the BHH hopping frequency, while in the lower panels it is doubled, keeping $\mathcal{E}/NU$ fixed. The color-code (from yellow to blue) corresponds to the trajectory-averaged occupation n (from $N/8$ to $N/2$).

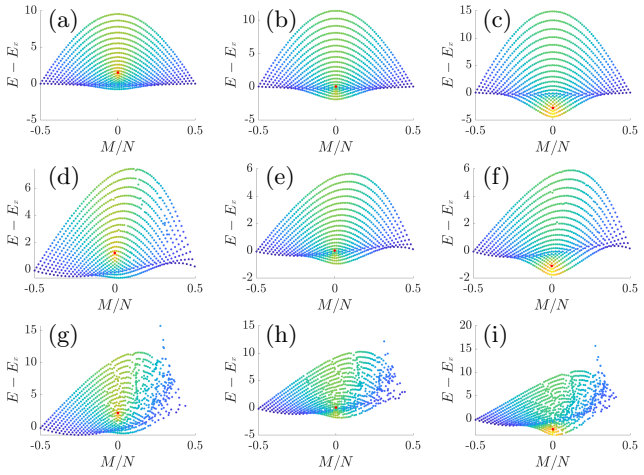

FIG. 5. **The spectrum.** The left to right arrangement of the panels is as in Fig.4. In the upper row we plot the spectrum of $\mathcal{H}^{(0)}$, while the two other rows provided the spectrum of $\mathcal{H}$ in one-to-one correspondence with Fig.4. All the spectra refer to ring with N=42 particles. The points are colored by the expectation value of n, with the same colorcode as in Fig.1 and Fig.4.

volution the generators $H_1 = \mathcal{H}^{(0)}$ and $H_2 = M$. The trajectories that are generated for a given E and M form a torus. Any point on the torus is accessible by generating a walk of duration (t_1, t_2). Consider the projected dynamics in (φ, n). A given trajectory has a period T, but in the full phase-space it is, in general, not periodic, because ϕ has advanced some distance β. It follows that in order to get a periodic walk on the torus, the $t_1 = T$ evolution that is generated by H_1, should be followed by a $t_2 = -\beta$ evolution that is generated by H_2. The so called rotation angle, β, characterizes the torus, and is imaged in Fig.1a [f]. Note that a $t_2 = 4\pi$ evolution that is generated by $H_2 = M$ is a periodic trajectory in phase space, because it does not affect the (φ, n) degree of freedom. We conclude that the set of periodic walks form a so called Arnold-Liouvile lattice, that can be spanned by the units vectors

$$\vec{\tau}_a = (T, -\beta) \tag{4}$$

$$\vec{\tau}_b = (0, 4\pi) \tag{5}$$

Let us now go back to Fig. 1a, where we plot β as a function of M and E. One can immediately spot the location of the pinched torus $(M, E) = 0$, around which β has 4π variation. Hence, after a parametric loop, we get the mapping $\vec{\tau}_a \mapsto \vec{\tau}_a - \vec{\tau}_b$ while $\vec{\tau}_b$ remains the same. Such non-trivial mapping is the hallmark of monodromy [11, 12]. Upon EBK quantization monodromy in the spectrum is implied [e]. This is demonstrated in the inset of Fig.1b. Namely, transporting an elementary unit cell (spanned by two basis vectors) around the pinched torus in the (M, E) spectrum, we end up with a different unit cell. Our spectrum is divided into two regions by the separatrix line, and therefore only the region with the pinched torus exhibits the non-trivial monodromy. At the swap transition the pinched torus and hence the non-trivial monodromy is relocated to the other region. In the special case of $\mathcal{E} = 0$, the pinched torus merges with the separatrix line, leaving both regions with a trivial monodromy.

Summary.– Several themes combine is the study of superflow metastability. There is a monodromy that is associated with the existence of the condensate; and another separatrix that is associated with the depleted states. They provide a classical skeleton for the many-body quantum spectrum. Chaos blurs the ordered spectrum, but the topological aspect remains robust. If the rotation frequency of the device is adjusted (detuning), a stochastic pathway is formed at the swap transition, leading to the depletion of the condensate, and the decay of the superflow. The analysis is relevant for future hysteresis-type experiments [23] with ring lattice circuits [27, 28].

Acknowledgements.– This research was supported by the Israel Science Foundation (Grant No.283/18)

[1] Maya Chuchem, Katrina Smith-Mannschott, Moritz Hiller, Tsampikos Kottos, Amichay Vardi, and Doron Cohen, "Quantum dynamics in the bosonic josephson junction," Phys. Rev. A **82**, 053617 (2010).

[2] Michael Albiez, Rudolf Gati, Jonas Fölling, Stefan Hunsmann, Matteo Cristiani, and Markus K. Oberthaler, "Direct observation of tunneling and nonlinear self-trapping in a single bosonic josephson junction," Phys. Rev. Lett. **95**, 010402 (2005).

[3] S Levy, E Lahoud, I Shomroni, and J Steinhauer, "The ac and dc josephson effects in a bose–einstein condensate," Nature **449**, 579–583 (2007).

[4] Luigi Amico, Davit Aghamalyan, Filip Auksztol, Herbert Crepaz, Rainer Dumke, and Leong Chuan Kwek, "Superfluid qubit systems with ring shaped optical lattices," Sci. Rep. **4**, 04298 (2014).

[5] Geva Arwas and Doron Cohen, "Superfluidity in bose-hubbard circuits," Phys. Rev. B **95**, 054505 (2017).

[6] Gh.-S. Paraoanu, "Persistent currents in a circular array of bose-einstein condensates," Phys. Rev. A **67**, 023607 (2003).

[7] David W Hallwood, Keith Burnett, and Jacob Dunningham, "Macroscopic superpositions of superfluid flows," New Journal of Physics **8**, 180–180 (2006).

[8] A Gallemí, M Guilleumas, J Martorell, R Mayol, A Polls, and Bruno Juliá-Díaz, "Fragmented condensation in bose–hubbard trimers with tunable tunnelling," New Journal of Physics **17**, 073014 (2015).

[9] Andrey R. Kolovsky, "Bosehubbard hamiltonian: Quantum chaos approach," International Journal of Modern Physics B **30**, 1630009 (2016).

[10] Geva Arwas, Amichay Vardi, and Doron Cohen, "Superfluidity and chaos in low dimensional circuits," Sci. Rep. **5**, 13433 (2015).

[11] J. J. Duistermaat, "On global action-angle coordinates," Communications on Pure and Applied Mathematics **33**, 687–706 (1980).

[12] Richard H Cushman and Larry M Bates, *Global aspects of classical integrable systems*, Vol. 94 (Springer, 1997).

[13] Richard Cushman and JJ Duistermaat, "The quantum mechanical spherical pendulum," Bulletin of the American Mathematical Society **19**, 475–479 (1988).

[14] San Vũ Ngoc, "Quantum monodromy in integrable systems," Communications in Mathematical Physics **203**, 465–479 (1999).

[15] B. Zhilinskii, "Hamiltonian monodromy as lattice defect," in *Topology in Condensed Matter*, edited by Michail Ilych Monastyrsky (Springer Berlin Heidelberg, Berlin, Heidelberg, 2006) pp. 165–186.

[16] K. Efstathiou, M. Joyeux, and D. A. Sadovskií, "Global bending quantum number and the absence of monodromy in the HCN ↔ CNH molecule," Phys. Rev. A **69**, 032504 (2004).

[17] R. H. Cushman, H. R. Dullin, A. Giacobbe, D. D. Holm, M. Joyeux, P. Lynch, D. A. Sadovskií, and B. I. Zhilinskií, "co_2 molecule as a quantum realization of the $1:1:2$ resonant swing-spring with monodromy," Phys. Rev. Lett. **93**, 024302 (2004).

[18] N. J. Fitch, C. A. Weidner, L. P. Parazzoli, H. R. Dullin, and H. J. Lewandowski, "Experimental demonstration of classical hamiltonian monodromy in the $1:1:2$ resonant elastic pendulum," Phys. Rev. Lett. **103**, 034301 (2009).

[19] Austen Lamacraft, "Spin-1 microcondensate in a magnetic field," Phys. Rev. A **83**, 033605 (2011).

[20] Michal Kloc, Pavel Strnsk, and Pavel Cejnar, "Monodromy in dicke superradiance," Journal of Physics A: Mathematical and Theoretical **50**, 315205 (2017).

[21] Holger R. Dullin and Holger Waalkens, "Defect in the joint spectrum of hydrogen due to monodromy," Phys. Rev. Lett. **120**, 020507 (2018).

[22] M. P. Nerem, D. Salmon, S. Aubin, and J. B. Delos, "Experimental observation of classical dynamical monodromy," Phys. Rev. Lett. **120**, 134301 (2018).

[23] Stephen Eckel, Jeffrey G. Lee, Fred Jendrzejewski, Noel Murray, Charles W. Clark, Christopher J. Lobb, William D. Phillips, Mark Edwards, and Gretchen K. Campbell, "Hysteresis in a quantized superfluid 'atomtronic' circuit," Nature **506**, 200–203 (2014).

[24] Oliver Morsch and Markus Oberthaler, "Dynamics of bose-einstein condensates in optical lattices," Rev. Mod. Phys. **78**, 179–215 (2006).

[25] Immanuel Bloch, Jean Dalibard, and Wilhelm Zwerger, "Many-body physics with ultracold gases," Rev. Mod. Phys. **80**, 885–964 (2008).

[26] Marcel Novaes, "Some basics of su (1, 1)," Revista Brasileira de Ensino de Fisica **26**, 351–357 (2004).

[27] Thomas A Bell, Jake A P Glidden, Leif Humbert, Michael W J Bromley, Simon A Haine, Matthew J Davis, Tyler W Neely, Mark A Baker, and Halina Rubinsztein-Dunlop, "Boseeinstein condensation in large time-averaged optical ring potentials," New journal of Physics **18**, 035003 (2016).

[28] M. Aidelsburger, J. L. Ville, R. Saint-Jalm, S. Nascimbène, J. Dalibard, and J. Beugnon, "Relaxation dynamics in the merging of n independent condensates," Phys. Rev. Lett. **119**, 190403 (2017).

[29] Alexander L. Fetter, "Rotating trapped bose-einstein condensates," Rev. Mod. Phys. **81**, 647–691 (2009).

[30] Y.-J. Lin, R. L. Compton, K. Jimenez-Garcia, J.V. Porto, and I. B. Spielman, "Synthetic magnetic fields for ultracold neutral atoms," Nature **462**, 628–632 (2009).

[31] J. Dalibard, F. Gerbier, G. Juzeliūnas, and P. Öhberg, "Colloquium: Artificial gauge potentials for neutral atoms," Rev. Mod. Phys. **83**, 1523 (2011)

.

[a] Supplementary Material - Section A. The Hamiltonian

[b] Supplementary Material - Section B. SPs and seperatrices; Stability analysis.

[c] Supplementary Material - Section C. Conical intersection perspective.

[d] Supplementary Material - Section D. Gallery: additional examples are provided.

[e] Supplementary Material - Section E. Hamiltonian Monondromy (pedagogical).

[f] Supplementary Material - Section F. The calculation of the phase β.

Monodromy and chaos for condensed bosons in optical lattices

Geva Arwas, Doron Cohen

SUPPLEMENTARY MATERIAL

A - The Hamiltonian

For L sites, in a ring geometry:

$$\mathcal{H} = \sum_{j=1}^{L}\left[\frac{U}{2}\boldsymbol{a}_j^\dagger\boldsymbol{a}_j^\dagger\boldsymbol{a}_j\boldsymbol{a}_j - \frac{K}{2}\left(\mathrm{e}^{i(\Phi/L)}\boldsymbol{a}_{j+1}^\dagger\boldsymbol{a}_j + \text{h.c.}\right)\right] \quad (6)$$

where K is the hopping frequency, U is the on-site interaction, and j mod(L) labels the sites of the ring. The $\boldsymbol{a}_j$ and $\boldsymbol{a}_j^\dagger$ are the Bosonic annihilation and creation operators. The total number of particles $N = \sum_j \boldsymbol{a}_j^\dagger\boldsymbol{a}_j$ is a constant of motion. The so-called Sagnac phase Φ is proportional to the rotation frequency of the device: it can be regarded as the Aharonov-Bohm flux that is associated with Coriolis field in the rotating frame [23, 29]. Optionally it can be realized as a geometric phase using artificial gauge fields [30, 31].

For a clean L-site ring lattice we define momentum orbitals whose wavenumbers are $k = (2\pi/L)\times$ integer. Consequently the BHH takes the form

$$\mathcal{H} \;=\; \sum_k \epsilon_k b_k^\dagger b_k \;+\; \frac{U}{2L}{\sum_{k_4}}' b_{k_4}^\dagger b_{k_3}^\dagger b_{k_2} b_{k_1} \quad (7)$$

where the prime implies the constraint $k_1+k_2+k_3+k_4 = 0$. Here $\epsilon_k = -K\cos(k-\Phi/L)$ are the single particle energies. Later we assume, without loss of generality, that the particles are initially condensed in the $k=0$ orbital. This is not necessarily the ground-state orbital, because we keep Φ as a free parameter.

For the purpose of semiclassical treatment we define action-angle variables via $b_k = \sqrt{n_k}e^{i\varphi_k}$. Taking into account that N is constant of motion, this Hamiltonian describes an $f = L-1$ freedoms system. If we had just two sites ($L=2$) the one-freedom Hamiltonian for the canonical variables $\tilde{n} = (n_1-n_0)/2$ and $\tilde{\varphi} = \varphi_1-\varphi_0$ would be

$$\mathcal{H}_{\text{dimer}}(\tilde{\varphi},\tilde{n}) = \mathcal{E}\tilde{n} + \frac{U}{2}\left(\frac{N^2}{4}-\tilde{n}^2\right)\left[1+\cos(2\tilde{\varphi})\right] \quad (8)$$

where $\mathcal{E} = \epsilon_1-\epsilon_0$, and an N dependent constant has been dropped. For $L=3$ site ring we have

$$\begin{aligned}\mathcal{H} \;&=\; \sum_{k=0,1,2}\epsilon_k n_k \;+\; \frac{U}{6}\sum_k n_k^2 \;+\; \frac{U}{3}\sum_{k'\neq k} n_{k'}n_k \quad (9)\\ &+\; \frac{U}{3}\sum_{k''\neq k'\neq k}\left[n_{k'}n_{k''}\right]^{1/2}\; n_k\;\cos\left(\varphi_{k''}+\varphi_{k'}-2\varphi_k\right)\end{aligned}$$

Also here we can define relative coordinates $q_1 = \varphi_1-\varphi_0$ and $q_2 = \varphi_2-\varphi_0$ where the subscripts refers to $k_{1,2} = \pm(2\pi/3)$. Defining $\mathcal{E}_k = (\epsilon_k-\epsilon_0)+(1/3)NU$ we get Eq.(1) with

$$\begin{aligned}\mathcal{H}^{(0)} \;&=\; \mathcal{E}_1 n_1 + \mathcal{E}_2 n_2 \;-\; \frac{U}{3}\left[n_1^2+n_2^2+n_1n_2\right]\\ &+\; \frac{2U}{3}(N-n_1-n_2)\sqrt{n_1n_2}\cos\left(q_1+q_2\right) \quad (10)\end{aligned}$$

and

$$\mathcal{H}^{(+)} \;=\; \frac{2U}{3}\sqrt{(N-n_1-n_2)n_1}\;n_2\cos\left(q_1-2q_2\right) \quad (11)$$

while $\mathcal{H}^{(-)}$ is obtained by swapping the indices $(1\leftrightarrow 2)$. In fact it is more convenient to use the coordinates

$$\begin{aligned}\phi[\text{mod}(4\pi)] \;&=\; q_1-q_2 \;=\; \varphi_1-\varphi_2\\ \varphi[\text{mod}(2\pi)] \;&=\; q_1+q_2 \;=\; \varphi_1+\varphi_2-2\varphi_0 \quad (12)\end{aligned}$$

and the conjugate coordinates

$$M \;=\; \frac{1}{2}(n_1-n_2) \;\in\left[-\frac{N}{2},\frac{N}{2}\right] \quad (13)$$

$$n \;=\; \frac{1}{2}(n_1+n_2) \;\in\left[|M|,\frac{N}{2}\right] \quad (14)$$

Then the Hamiltonian takes the form of Eq. (1) with Eq. (2) and Eq. (3), where the detuning is $\mathcal{E} = \mathcal{E}_1+\mathcal{E}_2-(1/2)NU$, and $\mathcal{E}_\perp = \mathcal{E}_1-\mathcal{E}_2$.

B - SPs and seperatrices

Consider a phase-space that is described by φ, n. We shall distinguish between *rotor geometry* for which the $n=0$ points are distinct, and *oscillator geometry* for which all the $n=0$ points are identified as one point. The algebraic treatment is the same, but the physical interpretation is different.

Regular point.– As an appetizer consider the Hamiltonian

$$H \;=\; \sqrt{2n}\sin(\varphi) \quad (15)$$

It looks singular at $n=0$, but in fact it is completely smooth there. Regarded as an oscillator it is canonically equivalent to $H=p$ that generates translations. Similar observation applies to the non-interacting dimer Hamiltonian $H = (1/2)(a_2^\dagger a_1 + \text{h.c.})$, which in action angle variables takes the form

$$H \;=\; \sqrt{\left(\frac{N}{2}-n\right)\left(\frac{N}{2}+n\right)}\;\cos(\varphi) \quad (16)$$

Here both the North and the South poles of the Bloch sphere ($n=\pm N/2$) are regular phase-space points, neither SP nor singular.

Stationary point.– Consider the standard quadratic Hamiltonian $H = (1/2)[ap^2 + bx^2]$. In polar canonical coordinates it is

$$H \;=\; [A + B\cos(2\varphi)]\;\; n \tag{17}$$

with $A = (a + b)$ and $B = (a - b)$. If $ab > 0$, equivalently $|A| > |B|$, the origin ($n = 0$) is an elliptic SP that is circled by trajectories that have the frequency

$$\omega \;=\; \sqrt{ab} \;=\; \sqrt{A^2 - B^2} \tag{18}$$

Otherwise the origin becomes an unstable hyperbolic SP. In the latter case there is an 8-like separatrix that goes through the origin: there are two ingoing directions and two outgoing directions. The approach to the SP along the separatrix, and its departure, is an infinitely slow motion.

Folded SP.– Consider the dimer Hamiltonian Eq.(8) with $2\tilde{\varphi}$ replaced by φ. Here the dynamics is the same from algebraic perspective, but the global geometry is different. It is a folded version of the dimer Hamiltonian. In the hyperbolic case the vicinity of the SP can be described as "half saddle". From local dynamics point of view the equations of motion are identical, but here the separatrix has only one outgoing direction and only one ingoing direction.

Spread SP.– Consider Eq.(17), but assume that we are dealing with rotor geometry. From local dynamics point of view the equations of motion are still identical, but now the arrival point (say φ_{in}) and the departure point (say φ_{out}) are not the same point.

Stability analysis.– Consider the Hamiltonian of Eq.(2) with $M = 0$. The origin ($n = 0$) is a *folded SP*. It is elliptic or hyperfolic depending on the detuning. Locally the Hamiltonian looks like Eq.(17) with

$$A = \mathcal{E} + \frac{NU}{2}, \qquad B = \frac{2NU}{3} \tag{19}$$

$$\text{SP unstable for} \quad -\frac{7NU}{6} < \mathcal{E} < \frac{NU}{6} \tag{20}$$

In the regime where the SP is stable the ω of Eq.(18) reflects the frequency of the Bogoliubov excitations [10]. In the hyperbolic case we have a separatrix that goes through the origin.

For the same Hamiltonian, the perimeter ($n = N/2$) is a *spread SP*. For the purpose of stability analysis we can identify the points along the perimeter as a single point of a Bloch sphere. Setting $\tilde{n} = N - 2n$ the Hamiltonian looks like Eq.(17) with

$$A = -\frac{\mathcal{E}}{2} + \frac{NU}{4}, \qquad B = \frac{NU}{3} \tag{21}$$

$$\text{SP unstable for} \quad -\frac{NU}{6} < \mathcal{E} < \frac{7NU}{6} \tag{22}$$

In the hyperbolic case we have a separatrix that meets the perimeter at one point and departs in a different point.

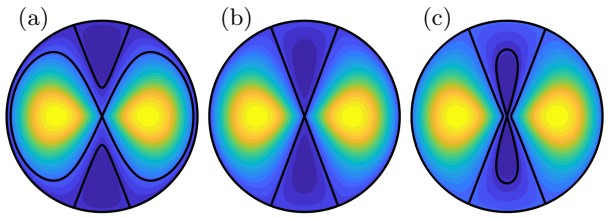

FIG. S1. Unfolded version of Fig.S3a that clarifies the notion of swap using polar coordinates $(\tilde{\varphi}, \tilde{n})$. If we identify all the points of the perimeter as a single point, we get the Bloch sphere of Fig.2b.

Combining with Eq.(20) we see that both SPs are unstable if $|\mathcal{E}| < (1/6)NU$. In the latter case we have two seperatrices. The separatrices swap as we go through $\mathcal{E} = 0$, see Fig.1.

Bloch sphere representation.– An unfolded version of Fig.2a is presented in Fig.S1. It should be emphasized that in the unfolded version each phase-space point is duplicated. Thanks to this duplication the separatrix that is associated with the central SP takes the familiar figure-8 saddle shape, which is more illuminating for illustration purpose. The Bloch spheres in Fig.2b is obtained if all the points along the perimeter are identified as a single point. Now also the perimeter separatrix takes the familiar figure-8 saddle shape. Using this physically unfaithful presentation it is easier to explain what do we mean by "swap of the separatrices". We note that the Poincare section in [10], that has been presented before we had proper understanding of the swap-transition, were physically unfaithful is the same sense.

The case of nonzero M**.**– For the same Hamiltonian Eq.(2) with $M \neq 0$, the points along the inner boundary $n = M$ are distinct. So we cannot regard them as a single point. Close to this inner boundary we have $H \sim \sqrt{\tilde{n}}\cos(\varphi)$, with $\tilde{n} = n - M$. This is a non-singular Hamiltonian, essentially the same as Eq.(15), that generates regular flow. It follows that the inner boundary is not special from a dynamical point of view: it can be regarded as *spread regular point*, it is not an SP, and there is no separatrix there.

The stability of the perimeter is determined as in Eq.(22), but with B multiplied by $\sqrt{1 - (2M/N)}$. Therefore, for sufficiently large M we always have $|A| > |B|$ and the perimeter is stable.

C - Conical intersection perspective

A useful way for visualizing the phase space tori is based on the $SU(1,1)$ symmetry [19, 26] of $\mathcal{H}^{(0)}$. For that we express the two conserved quantities, namely the energy E and the constant of motion M, in terms of the

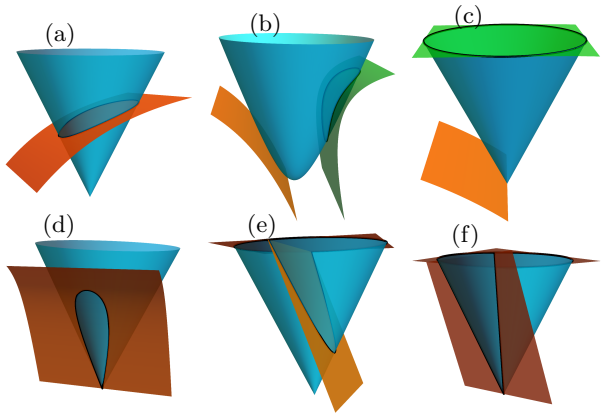

FIG. S2. Several examples of the reduced phase-space in the (K_x, K_y, K_z) coordinates (the symmetry axis is K_z). The blue cone (a,c-f) is the surface of constant $M = 0$ while the blue hyperbole (b) is the surface of constant $M = 0.15N$. The remaining surfaces correspond to a constant E. The intersection of constant M and E surfaces (highlighted in black) is a trajectory in the reduced (φ, n) space, and provides a useful way of visualizing the phase space tori (see text).

group generators. We start by introducing:

$$K_z = n + \frac{1}{2} \quad , \quad K_+ = a_1^\dagger a_2^\dagger \quad , \quad K_- = a_1 a_2 \quad (23)$$

which is a realization of the $SU(1,1)$ group, satisfying the algebra:

$$[K_z, K_\pm] = \pm K_\pm \quad , \quad [K_+, K_-] = -2K_z \quad (24)$$

The Casimir operator of the group, which commutes with all the generators, is:

$$C \;=\; K_z^2 - K_x^2 - K_y^2 \quad (25)$$

where K_x and K_y are given by $K_\pm = K_x \pm iK_y$. In the semiclassical treatment we have:

$$K_x \;\sim\; \sqrt{n_1 n_2}\cos\varphi \quad \in [-\Delta, \Delta] \quad (26)$$
$$K_y \;\sim\; \sqrt{n_1 n_2}\sin\varphi \quad \in [-\Delta, \Delta] \quad (27)$$
$$K_z \;\sim\; n \quad \in \left[|M|, \frac{N}{2}\right] \quad (28)$$

where $\Delta = \sqrt{(N/2)^2 - M^2}$. The Hamiltonian can be written in terms of the generators as:

$$\mathcal{H}^{(0)} \;=\; \mathcal{E}K_z + \mathcal{E}_\perp M - \frac{U}{3}M^2 + \frac{2U}{3}(N - 2K_z)\left[\frac{3}{4}K_z + K_x\right] \quad (29)$$

As for the constant of motion M, we have $M^2 = C$. In Fig.S2 we plot several examples for the M^2 and $\mathcal{H}^{(0)} = E$ surfaces in the (K_x, K_y, K_z) space. For $M = 0$ Eq.(25) defines a cone whose tip corresponds to $n = 0$, while its outer boundary to $n = N/2$. For for a constant $M \neq 0$ Eq.(25) defines an hyperboloid whose base corresponds to $n = |M|$, while its outer boundary to $n = N/2$.

The intersection between the E and M^2 surfaces is a trajectory in the reduced (φ, n) phase space. In the full phase space, we also have the phase ϕ, which dynamically changes as $\dot{\phi} = \partial\mathcal{H}/\partial M$. If the intersection between the surfaces forms a closed loop, as in Fig.S2(a,b), the dynamics in the full (φ, ϕ, n, M) phase-space covers a 2-torus (which is, of course, the typical case in an integrable 2 DOF system). When the two surfaces tangent, as in Fig.S2(b), the trajectory is a fixed point in the (φ, n) space, and a circle in the full phase space.

Trajectories that pass through $n = 0$ should be addressed with more caution. As explained in the main text, the tip of the cone does not correspond to a ϕ circle, but to a single point. This is because $n = 0$ means $n_1 = n_2 = 0$ so that ϕ is degenerate. When the $n = 0$ SP is stable, the energy surface is tangent to the tip of the cone, as in Fig.S2(c), hence the trajectory is a single point in phase space. When unstable, the intersection forms a cusped circle, see Fig.S2(d), representing a *pinched torus*, i.e. a torus with one of its ϕ circles shrinks to a point.

Trajectories that pass through $n = N/2$ are special too. When the $n = N/2$ SP is stable, as in Fig.S2(c), the intersection is the entire outer circle of the cone, reflecting the fact that it is a *spread* SP. When unstable, see Fig.S2(e), a separatrix trajectory is formed, which meets the $n = N/2$ circle at two points, corresponding to φ_{in} and φ_{out}. At the swap transition, the two SPs are connected, i.e. the cusped circle of $n = 0$ merged with the separatrix trajectory of $n = N/2$, as shown in Fig.S2(f).

D - Gallery

In the main text of the Ms we have focused on the regime where both SPs are unstable. Here we provide phase space plots and spectra for the whole range of the detuning parameter. Fig. S3 is an extended version of Fig.2, and Fig.S4 is an extended version of Fig.5.

E - Hamiltonian Monondromy

Consider generators (H_1, H_2) in involution, i.e. that commute with each other. The generated trajectories are moving on an energy surface labeled (E_1, E_2). A *walk* consists of t_1 evolution using H_1, and t_2 evolution using H_2. The involution implies that the walks are commutative. Accordingly the parameterization of a walk is $\vec{t} = (t_1, t_2)$. Periodic walk is a walk that brings you back to the same point. The set of periodic walks forms a lattice in $\vec{t}$ space. This lattice is spanned by basis vectors $\vec{\tau}_k$, where $k = a, b$. We can formally write any point in $\vec{t}$

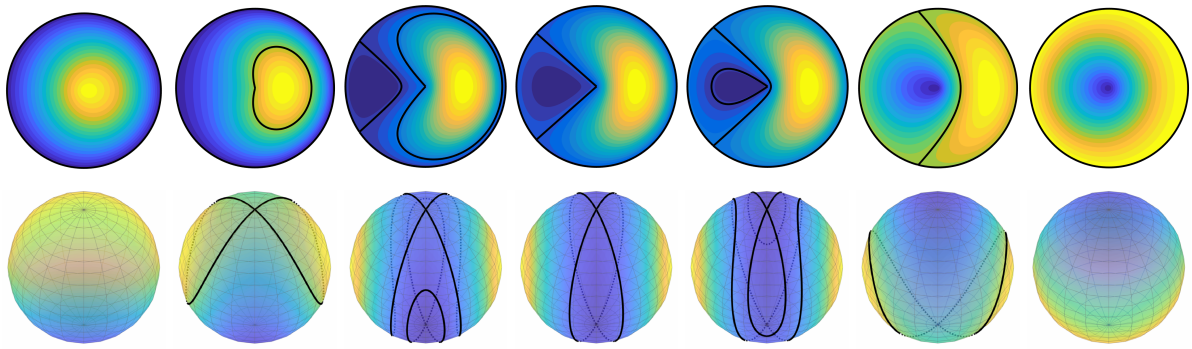

FIG. S3. **The geometry of the projected phase space.** Top panels: the (φ, n) disk. Bottom panels: the $(\tilde{\varphi}, \tilde{n})$ Bloch-sphere. The detuning from left to right is $\mathcal{E}/NU = -4/3, -1/3, -0.05, 0, 0.05, 1/3, 4/3$. The contours are color-coded by the energy of the trajectories. The black curves are seperatrices that pass through the SPs.

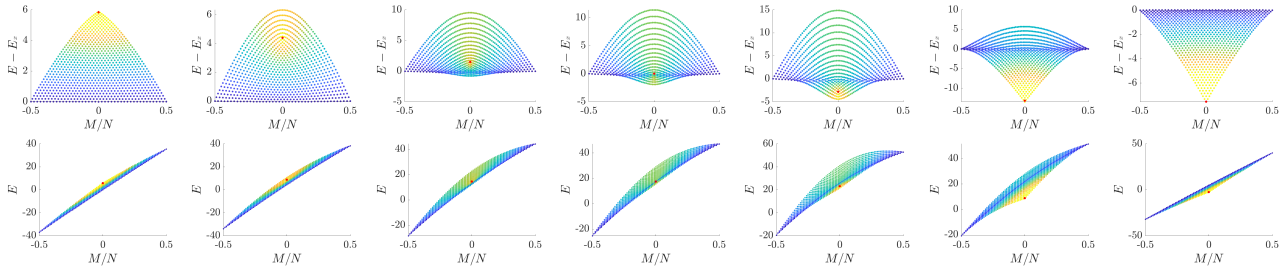

FIG. S4. **The spectrum.** The top row panels are the spectrum of $\mathcal{H}^{(0)}$ with the same $\mathcal{E}/NU$ values as in Fig.S3. In the bottom row the same spectra is plotted, but without subtracting the separatrix energy. The interaction strength from left to right is $NU \approx 0.2, 0.6, 1.4, 1.9, 2.7, 1.9, 0.3$ in units of the BHH hopping frequency K. Note that for the top row panels, different NU values will produce the same plot and only scale the $E - E_x$ axis. Note that the energy here differs by a constant from Fig.1(b).

space as

$$\vec{t} \;=\; \sum_k \frac{\theta_k}{2\pi}\vec{\tau}_k \;=\; \frac{\theta_a}{2\pi}\vec{\tau}_a + \frac{\theta_b}{2\pi}\vec{\tau}_b \tag{30}$$

We define a reciprocal basis such that

$$\vec{\omega}_k \cdot \vec{\tau}_{k'} \;=\; 2\pi\delta_{k,k'} \tag{31}$$

The reciprocal relation is

$$\theta_k \;=\; \vec{\omega}_k \cdot \vec{t} \tag{32}$$

Once action variables are defined we have

$$\vec{\omega}_k \;=\; \left(\frac{\partial H_1}{\partial J_k}, \frac{\partial H_2}{\partial J_k}\right) \tag{33}$$

The spacings between two energies is

$$\Delta E \;=\; \sum_k \vec{\omega}_k \cdot \overrightarrow{\Delta n}_k \tag{34}$$

Thus the spectrum forms a reciprocal lattice.

Considering a closed loop in (E_1, E_2) space, the monodromy matrix is defined as the mapping

$$\vec{\tau}_k(\text{final}) \;=\; \sum_l \mathbf{M}_{kl}\vec{\tau}_l \tag{35}$$

If the loop encircles a pinched torus we have [12]

$$\mathbf{M} \;=\; \begin{pmatrix} 1 & -1 \\ 0 & 1 \end{pmatrix} \tag{36}$$

so we get the mapping $\vec{\tau}_a \mapsto \vec{\tau}_a - \vec{\tau}_b$, as discussed in the main text after Eq.(4). For the reciprocal basis we have:

$$\vec{\omega}_k(\text{final}) \;=\; \sum_l \tilde{\mathbf{M}}_{kl}\,\vec{\omega}_l \tag{37}$$

where $\tilde{\mathbf{M}} = [\mathbf{M}^{-1}]^t$. This can be seen by writing:

$$\begin{aligned} 2\pi\delta_{k,k'} \;&=\; [\vec{\omega}_k(\text{final})] \cdot [\vec{\tau}_{k'}(\text{final})] \\ &= \sum_{lm} \tilde{\mathbf{M}}_{kl}\mathbf{M}_{k'm}\;\vec{\omega}_i \cdot \vec{\tau}_j \;=\; 2\pi \sum_l \tilde{\mathbf{M}}_{kl}\mathbf{M}_{k'l} \end{aligned} \tag{38}$$

hence $\tilde{\mathbf{M}}\mathbf{M}^t = \mathbf{1}$ and $\tilde{\mathbf{M}} = [\mathbf{M}^{-1}]^t$. For a loop which encircles the pinched torus we then have

$$\tilde{\mathbf{M}} \;=\; \begin{pmatrix} 1 & 0 \\ 1 & 1 \end{pmatrix} \tag{39}$$

which reflects the way $\vec{\omega}_k$ are mapped, and therefore how a unit cell in the quantum spectrum is transformed, as seen in Fig.1(b).

F - The calculation of the phase β

Some technical remarks are in order regarding the T and the β determination in Eq.(4). For nonzero winding number the phase-space torus loops around φ. This is like rotation-motion of a pendulum. For a zero winding number the phase-space torus does not see the topology of φ. This is like libration-motion of a pendulum. For rotation, T is defined as the time at which $\varphi(t)$ comes back to the initial value $\varphi(0)$. For libration, that has the same period, the phase $\varphi(t)$ crosses twice $\varphi(0)$, but with different momentum n. If we gradually change the energy, we go from libration to rotation. The numerical definition of β should take into account the change of topology. At the point of the crossover $T \to \infty$, while β is ill-defined.

Additional remark is in order regarding the determination of the 4π in Eq. (5). It should be clear that the original phases $(\varphi_0, \varphi_1, \varphi_2)$ are defined $\mod(2\pi)$. Next we define the coordinates $q_1 = \varphi_1 - \varphi_0$ and $q_2 = \varphi_2 - \varphi_0$, and the alternate coordinates $\phi = q_1 - q_2$ and $\varphi = q_1 + q_2$. If the alternate coordinates are regarded as $\mod(2\pi)$ angles, it follows that each (φ, ϕ) represent *two* points in q space, and each (φ, n) in our sections is the projection of a 4π circle. Consider a trajectory that is generated using $H_2 = M$. In the (φ_1, φ_2) torus it will have a constant φ. You will have to run t a 4π interval in order to get back to the starting point.